A Statistical Model for Indoor Multipath Propagation

ADEL A. M. SALEH, FELLOW, IEEE, AND REINALDO A. VALENZUELA, MEMBER, IEEE

Abstract—**The results of indoor multipath propagation measurements using 10 ns, 1.5 GHz, radarlike pulses are presented for a medium-size office building. The observed channel was very slowly time varying, with the delay spread extending over a range up to about 200 ns and rms values of up to about 50 ns. The attenuation varied over a 60 dB dynamic range. A simple statistical multipath model of the indoor radio channel is also presented, which fits our measurements well, and more importantly, appears to be extendable to other buildings. With this model, the received signal rays arrive in clusters. The rays have independent uniform phases, and independent Rayleigh amplitudes with variances that decay exponentially with cluster and ray delays. The clusters, and the rays within the cluster, form Poisson arrival processes with different, but fixed, rates. The clusters are formed by the building superstructure, while the individual rays are formed by objects in the vicinities of the transmitter and the receiver.**

I. INTRODUCTION

THE use of radio for indoor data or voice communications, e.g., within an office building, a warehouse, a factory, a hospital, a convention center, or an apartment building, is an attractive proposition. It would free the users from the cords tying them to particular locations within these buildings, thus offering true mobility, which is convenient and sometimes even necessary. It would also drastically reduce wiring in a new building, and would provide the flexibility of changing or creating various communications services in existing buildings without the need for expensive, time-consuming rewiring. The challenge is to offer such services to the majority of the people in a building, not just a selected few. This would most certainly involve a sophisticated local radio communications system whose engineering would require the knowledge of the spatial and temporal statistics of the signal attenuation, the multipath delay spread, and even the impulse response of the indoor radio channel involved.

Various measurements have been reported in the literature for the attenuation of microwave CW signals propagating within buildings [1], [2] or into buildings [3]–[6]. The work of Alexander given in [2], which was done at 900 MHz, is particularly useful since it gives the power law representing the signal attenuation as a function of distance for various types of building.

The first multipath delay spread measurements within a building were reported recently by Devasirvatham [7]. He used a carrier at 850 MHz, biphase-modulated with a 40 Mbit/s maximal-length pseudonoise code, resulting in a 25 ns time resolution. The measurements were made in a large office building (AT&T Bell Laboratories main location in Holmdel, NJ), which occupies an area of 315 × 110 m and is 6 stories high.

In the present paper, we present the results of multipath delay spread and attenuation measurements within a medium-size two-story office building (AT&T Bell Laboratories, Crawford Hill location in Holmdel, NJ), whose first floor plan is sketched in Fig. 1. The external walls of this building are made of steel beams and glass, while the internal walls are almost entirely made of wood studs covered with plasterboard. The rooms contained typical metal office furniture and/or laboratory equipment. The measurements were made by using low-power 1.5 GHz radarlike pulses to obtain a large ensemble of the channel's impulse responses with a time resolution of about 5 ns. Based on these measurements, as well as some of the others cited above, we propose a statistical model of the indoor radio channel, which 1) has enough flexibility to permit reasonably accurate fitting of the measured channel responses, 2) is simple enough to use in simulation and analysis of various indoor communications schemes, and 3) appears to be extendable (by adjusting its parameters) to represent the channel within other buildings.

II. MEASUREMENT SETUP

A schematic diagram of the measurement setup is shown in Fig. 2. An RF sweep oscillator was used to generate a 1.5 GHz CW signal, which was then modulated by a train of 10 ns pulses with 600 ns repetition period, which is longer than any delay observed in the test building. This radarlike signal was amplified and transmitted via a vertically polarized discone antenna [8] whose radiation pattern is omnidirectional in the horizontal plane. The discone was chosen over a vertical dipole, which has an almost identical radiation pattern, because of its superior bandwidth, which provided the flexibility of changing or sweeping the signaling frequency when desired. The average transmitted power could be adjusted with a step attenuator over a range from a fraction of a nanowatt to several milliwatts.

At the receiver, a second vertically polarized discone antenna was used followed by a low-noise (3 dB noise figure) FET amplifier chain with a 60-dB gain over a frequency range of 1 to 2 GHz. (Actually, the state of polarization of the receiving antenna did not matter from a statistical viewpoint.) The signal was then detected with a sensitive square-law envelope detector whose output was displayed on a computer-controlled digital storage oscil-

Manuscript received January 23, 1986; revised September 24, 1986.

The authors are with AT&T Bell Laboratories, Crawford Hill Laboratory, Holmdel, NJ 07733.

IEEE Log Number 8612162.

0733-8716/87/0200-0128$01.00 © 1987 IEEE

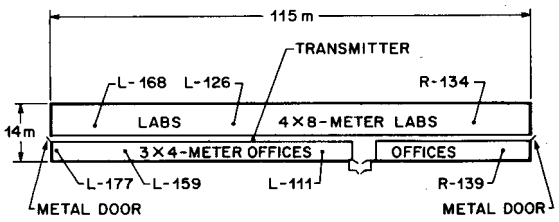

Fig. 1. Plan of the first floor of AT&T Bell Laboratories' Crawford Hill building in Holmdel, NJ.

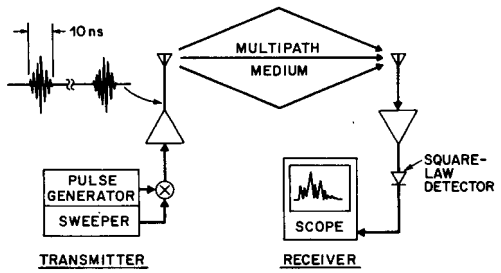

Fig. 2. A schematic representation of the measurements setup.

loscope (Tektronix model 7854). The dynamic range of our setup was more than 90 dB, which was achieved by manually adjusting the step attenuator at the transmitter as well as the oscilloscope's vertical gain.

The transmitter was fixed in the hallway near the center of the first floor of the building (see Fig. 1) with its antenna located at a height of about 2 m. The receiver, with the antenna at the same height, was moved to collect measurements in the hallway and in several rooms throughout the same floor. (No floor-to-floor penetration measurements are presented since the signal level in that case was generally too small to detect with our setup.) A total of 8 rooms were measured with about 25 pulse responses at various locations within each room. Both the transmitter and the receiver were stationary during the acquisition of each pulse response. For reasons to be explained in the next section, the transmitted signal frequency was swept at a rate of about 100 Hz over $\pm$ 100 MHz around the 1.5-GHz center frequency. The waveform processing capability of the oscilloscope was used to average the received frequency-swept pulse responses, and to transfer that average to a computer for storage. The averaging process took about 15 s to complete. To freeze the channel during that time, we made sure that people in the vicinity of the transmitting and receiving antennas, or those in the hallway between the antennas, stopped moving. (People moving within their offices, or in other locations in and around the building, had a negligible effect on the measurements.) A coaxial cable was used to trigger the oscilloscope from the transmitter's pulse generator to guarantee a stable timing reference under our swept conditions.

III. Mathematical Formulation of the Method of Measurements

Each transmitted RF radarlike pulse has the complex time domain representation

$$x(t) = p(t)\, e^{j(\omega t + \phi)}, \tag{1}$$

where $p(t)$ is the baseband pulse shape (which in our case has a width of about 10 ns), ω is the RF angular frequency (which is nominally $2\pi \times 1.5$ GHz in our experiment), and ϕ is an arbitrary phase.

The channel is represented by multiple paths or rays having real positive gains $\{\beta_k\}$, propagation delays $\{\tau_k\}$, and associated phase shifts $\{\theta_k\}$, where k is the path index; in principle, k extends from 0 to ∞. Thus, the complex, low-pass channel impulse response is given by [9]

$$h(t) = \sum_k \beta_k e^{j\theta_k} \delta(t - \tau_k), \tag{2}$$

where $\delta(\cdot)$ is the Dirac delta function.

Because of the motion of people and equipment in and around the building, the parameters β_k, τ_k, and θ_k are randomly time-varying functions. However, the rate of their variations is very slow compared to any useful signaling rates that are likely to be considered, e.g., higher than tens of kbit/s. Thus, these parameters can be treated as virtually time-invariant random variables.

It follows from (1) and (2) that the received signal, which is the time convolution of $x(t)$ and $h(t)$, is given by

$$y(t) = \sum_k \beta_k p(t - \tau_k)\, e^{j[\omega(t-\tau_k) + \phi + \theta_k]}. \tag{3}$$

Upon passing through the square-law envelope detector, as indicated in Fig. 2, the power profile displayed on the oscilloscope becomes

$$|y(t)|^2 = \sum_k \sum_l \left\{ \beta_k \beta_l p(t - \tau_k)\, p(t - \tau_l) \cdot e^{j[\theta_k - \theta_l + \omega(\tau_l - \tau_k)]} \right\}. \tag{4}$$

If there were no overlap of pulses, i.e., in our experiments, if $|\tau_k - \tau_l| \geq 10$ ns when $k \neq l$, then (4) would have reduced to

$$|y(t)|^2 = \sum_k \beta_k^2 p^2(t - \tau_k), \quad \text{no overlap}, \tag{5}$$

which is much simpler to use than (4) in estimating the β's and the τ's from the measured $|y(t)|^2$ waveform.

To obtain the simplification of (5) even with pulse overlap, we make the reasonable assumption that the θ's are statistically independent uniform random variables over $[0, 2\pi)$. In this case, the mathematical expectation of (4) with respect to the θ's yields

$$E_\theta\left\{ |y(t)|^2 \right\} = \sum_k \beta_k^2 p^2(t - \tau_k), \tag{6}$$

which is identical to (5) but allows for pulse overlap.

The mathematical expectation with respect to the θ's was, in effect, accomplished in our experiment by averaging the oscilloscope's power waveform while sweeping the transmitted RF frequency. Indeed, if the total swept bandwidth Δf is sufficiently large, it can be shown using

(4) that the frequency-average power profile is given by

$$s(t) \equiv \frac{1}{\Delta f}\int_{-\Delta f/2}^{\Delta f/2} \left| y(t)\right|^2 df \approx \sum_k \beta_k^2 p^2(t-\tau_k). \quad (7)$$

In our case, $\Delta f = 200$ MHz, which is sufficient to satisfy (7) for pulses that are separated by more than about 4 ns. Thus, overlapping pulses of closer separation could not be resolved and were considered to belong to "one path."

Given a frequency-averaged power profile $s(t)$, and knowing the shape of the transmitted pulse $p(t)$, we need to find pairs $\{(\tau_k, \beta_k^2), k = 1, 2, 3, \cdots\}$ that fit (7) under some minimum error criterion. A reasonable way of doing this is by picking $\{\tau_k\}$ to represent discrete points on the time axis, say, every 1–5 ns, then proceeding to find the corresponding $\{\beta_k^2\}$ to minimize the mean-square error involved in fitting (7) under the constraint that $\beta_k^2 \geq 0$, all k. This is a classic problem in *quadratic programming*, whose rigorous automated solution is somewhat involved. Because of the limited number of waveforms that we had to process (8 rooms times 25 profiles per room), we actually performed an interactive heuristic computer optimization. The resulting errors were still within the measurement uncertainty.

IV. Review of Measured Responses

A typical sequence of pulse responses involved in measuring a room is shown in Fig. 3. Actually, the responses shown are frequency-averaged power profiles, $s(t)$, as defined in (7). In all cases, the horizontal time axis covers 10 ns per division, the vertical axis is linear in power (not decibels), and the vertical sensitivity of the oscilloscope is left unchanged. The dB numbers shown in the various figures corresponds to the setting of the transmitter's step attenuator.

Fig. 3(a) shows the squared envelope of the transmitted pulse obtained by a direct coaxial connection between transmitter and receiver. In Fig. 3(b), the receiving and transmitting antennas are both located in the hallway at a 1-m separation. Some pulse broadening is observed, and the peak signal level has dropped by about 34 dB. This is only 2 dB more than the theoretical free-space power transmission ratio [10]

$$P_{\text{rec}}/P_{\text{trans}} = G_t G_r [\lambda_0/4\pi r]^2, \quad (8)$$

where G_t and G_r (≈ 1.6) are, respectively, the gains of the transmitting and receiving discone antennas, λ_0 ($= 0.2m$) is the RF wavelength, and r ($= 1m$) is the antenna separation. Note that, within a building, this relation is expected to hold only for small r, where the direct line-of-sight ray dominates all other rays.

Fig. 3(c) is obtained by moving the receiver about 60 m, still in the hallway directly in front of the room in question (R-139 in Fig. 1). A strong 60 ns echo now exists, which was found to occur as a result of a reflected wave from the metal door in the right-hand side of Fig. 1. The signal level dropped from the previous 1-m location by about 30 dB.

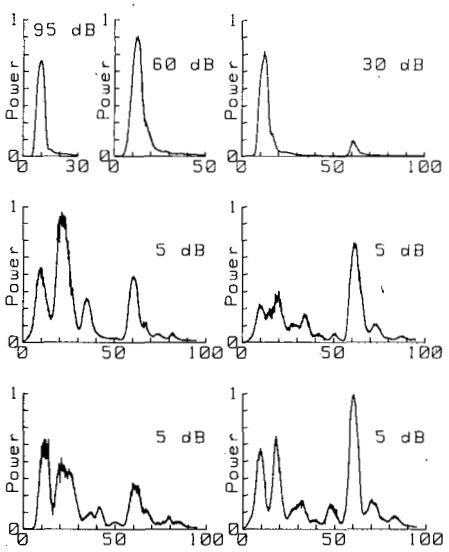

Fig. 3. A sample sequence of frequency-averaged power-profile measurements. The dB figures represent settings of the transmitter's attenuator.

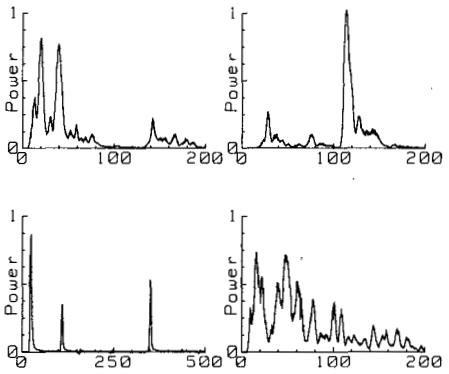

Fig. 4. Four interesting examples of frequency-averaged power profiles.

Fig. 3(d)–(g) corresponds to four measurements inside the room on the vertices of a 0.23-m square (9-in tile). The received echos now extend over about 100 ns, and the signal level has dropped by an additional 25 dB relative to the previous location in the hallway. Notice some spatial correlation among the four profiles. Notice also that the groups of rays starting at about 60 ns in Fig. 3(d)–(g) coincide with the small echo in Fig. 3(c), which is taken in the hallway just outside the room.

Fig. 4 shows four other measured pulse responses in different locations within the building. Fig. 4(a) (Room L-159 in Fig. 1) shows two clearly separated clusters of arriving rays covering a 200 ns time span. Fig. 4(b) (Room R-134 in Fig. 1) shows a 100 ns delayed echo that is much stronger than the first arriving rays. Fig. 4(c) (hallway in front of Room R-134 in Fig. 1) shows a strong echo that is delayed about 325 ns, which is the largest delay of a relevant echo that we observed. Fig. 4(d) corresponds to measurements done where both transmitter and receiver

were on the second floor of the building, with the receiver located in a large ($\approx 13 \times 17$ m) open machine shop with cinder-block surrounding walls. Notice the high density of the received rays over the entire 200 ns time axis.

V. The Multipath Power Gain and rms Delay Spread

A. Definitions

Getting the set of pairs $\{(\tau_k, \beta_k)\}$, as defined in (2), and deducing their joint statistics is, of course, the ultimate desired result of modeling. However, there are two simple parameters that are useful in describing the overall characteristics of the multipath profile. These are the total *multipath power gain*

$$G \equiv \sum_k \beta_k^2, \tag{9}$$

which is actually less than unity, and the *rms delay spread* [11]

$$\sigma_\tau \equiv \sqrt{\overline{\tau^2} - (\overline{\tau})^2}, \tag{10}$$

where

$$\overline{\tau^n} \equiv \frac{\sum_k \tau_k^n \beta_k^2}{\sum_k \beta_k^2}, \qquad n = 1, 2. \tag{11}$$

The power gain is useful in estimating such things as the signal-to-noise ratio of a communications system. The rms delay spread is a measure of the temporal extent of the multipath delay profile, which relates to performance degradation caused by intersymbol interference. In fact, in some communications systems with data rates small compared to $1/\sigma_\tau$, σ_τ is found to be the most important single parameter determining the performance [12]. This, however, is not true in general [12].

The above parameters can actually be obtained directly from the received frequency-averaged power profile, $s(t)$ defined in (7), without the need to know the individual β's and τ's. Define the received power profile moments

$$M_n \equiv \int_{-\infty}^{\infty} t^n s(t)\, dt, \qquad n = 0, 1, 2, \tag{12}$$

the transmitted pulse moments,

$$m_n \equiv \int_{-\infty}^{\infty} t^n p^2(t)\, dt, \qquad n = 0, 1, 2, \tag{13}$$

the corresponding averages

$$\overline{t_s^n} = M_n/M_0, \qquad n = 1,2, \tag{14}$$

$$\overline{t_p^n} = m_n/m_0, \qquad n = 1,2, \tag{15}$$

and the variances

$$\sigma_s^2 = \overline{t_s^2} - (\overline{t_s})^2, \tag{16}$$

$$\sigma_p^2 = \overline{t_p^2} - (\overline{t_p})^2. \tag{17}$$

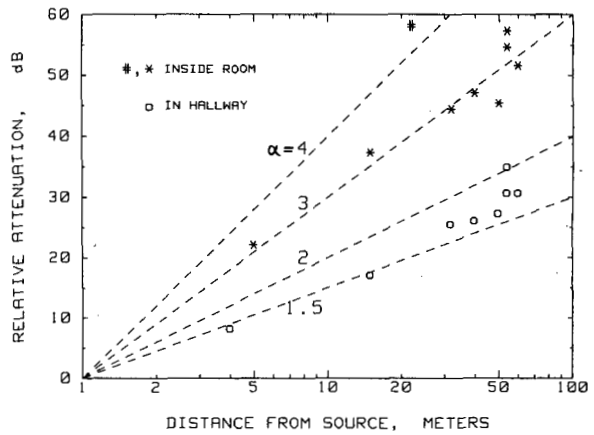

Fig. 5. Measured signal attenuation versus distance relative to 1-m separation. The dashed lines are for different values of the distance-power law exponent.

It can be shown that

$$G = M_0/m_0, \tag{18}$$

$$\overline{\tau} = \overline{t_s} - \overline{t_p}, \tag{19}$$

$$\sigma_\tau^2 = \sigma_s^2 - \sigma_p^2. \tag{20}$$

Note that G and σ_τ, but not $\overline{\tau}$, are independent of the choice of the time origin.

B. Distance-Power Law

The spatial average value $\overline{G}$ of the multipath power gain in the neighborhood of a point at a distance r from the transmitter is, in general, a decreasing function of r. Usually, this function is represented by a distance-power law of the form.

$$\overline{G}(r) \sim r^{-\alpha}. \tag{21}$$

In free space, $\alpha = 2$, and the power gain obeys an inverse-square law as given by (8).

A logarithmic plot of our measured attenuation

$$L(r) = -10 \log_{10} [G(r)/G(1 \text{ m})], \tag{22}$$

in decibels, versus r, in meters, is given in Fig. 5. Note that $G(1 \text{ m})$ can be computed reasonably accurately from (8).

Each rounded square in Fig. 5 represents one measurement with the receiver located in the same hallway as the transmitter. These measurements obey a power-law relation with $\alpha < 2$, which is the result of a waveguiding effect. Each asterisk in Fig. 5 represents the average of about 20 points within a room at the indicated distance from the transmitter. Recall, from Fig. 1, that all the rooms are located off the same hallway containing the transmitter. The value $\alpha = 3$ fits our room measurements reasonably well.

The single point indicated by the sharp sign in Fig. 5 represents the average of about 20 measurements where both the transmitter and the receiver were in the second floor of the building, with the receiver located in a large

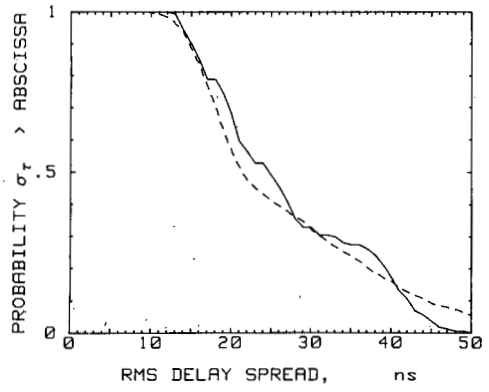

Fig. 6. Measured cumulative probability distribution of the rms delay spread for all rooms (solid line), and the result of a simulation using our model (dashed line).

open machine shop with cinder-block surrounding walls [same room as that for Fig. 4(d)]. Unlike the one-dimensional hallway geometry of Fig. 1, the shop in this case was located off a second hallway that is perpendicular to the transmitter's hallway. This resulted in a value of α slightly larger than 4. This is in more general agreement with Alexander's results [2] for this type of building. According to him, α can even be as large as 6 for office buildings with metalized partitions. (In a recent conference, Murray, Arnold, and Cox [19] reported on values of α between 3 and 4 measured in our building at 815 MHz.)

C. Statistics of the rms Delay Spread

Our measured rms delay spread, σ_τ, within the individual rooms was not generally correlated with the distance to the transmitter as had been previously predicted by Schmid [13]. Rather, it was somewhat related to the local surroundings of the transmitter and the receiver, e.g., to their proximity to such large reflectors as the end metal doors in Fig. 1. This is more consistent with the result of Turin *et al.* [14] of the urban mobile-radio channel.

The combined cumulative distribution of σ_τ resulting from a total of about 150 measurements within 7 rooms on the first floor of the building (see Fig. 1) is plotted by the solid line in Fig. 6. The results indicate that the rms delay spread has a median value of about 25 ns and a maximum value of about 50 ns. These numbers are a factor of five less than those measured by Devasirvatham in a much larger office building [7]. (In a recent conference, Devasirvatham [20] reported on rms delay spread of up to 200 ns measured in our building at 850 MHz. This large value, however, occurred only when the received signal levels were extremely low, e.g., 100–140 dB of path loss. When he truncated the data to a subset having path loss less than 100 dB, as is the situation in our case, he obtained results comparable to ours.)

We did not include in Fig. 6 the handful of measurement taken in the hallway, which occasionally yielded values of σ_τ much larger than 50 ns. For example, the measurement of Fig. 4(c) corresponds to $\sigma_\tau \approx 150$ ns. In fact, hallway measurements were excluded from our model development process altogether because, unlike room measurements, they include a direct line-of-sight ray from transmitter to receiver as well as strong rays with long delays, which is not the typical situation in most office buildings.

VI. Proposed Model

A. Basic Conjectures

We employ the discrete representation of the channel's impulse response given by (2). As mentioned earlier, the phase angles $\{\theta_k\}$ will be assumed *a priori* to be statistically independent random variables with a uniform distribution over $[0, 2\pi)$. We believe that this is self-evident and needs no experimental justification. Our goal now is to find the joint statistics of the paths gains $\{\beta_k\}$ and arrival times $\{\tau_k\}$.

We start with the attractive conjecture, which was pioneered by Turin *et al.* [14] in modeling urban mobile-radio channels, that $\{\tau_k\}$ forms a Poisson arrival-time sequence with some mean arrival rate λ. The path gain β_k associated with every τ_k is then picked from some probability distribution whose moments (e.g., mean and mean square) are functions of τ_k that eventually vanishes for large values of τ_k.

For simplicity, it would be desirable to have a model with λ being a constant and the β's statistically independent from one another. A straightforward implementation of these features, however, can lead to inconsistency with our experimental observations, as will be discussed next.

B. Clustering of Rays

Observations of measured pulse responses, such as some of those given in Figs. 3 and 4, indicate that rays generally arrive in clusters. Similar observations were found in the experimental data of Turin *et al.* [14]. This is clearly not consistent with a simple Poisson arrival-time model with constant λ. Indeed, Turin *et al.* as well as subsequent researchers [15], [16] who further refined their work, abandoned this model in favor of a Markov-type model in which the time axis is, in effect, divided into "bins," with the probability of a ray arriving within a given bin related to whether or not a ray actually arrived in the previous bin. Furthermore, in their model, the path gains in successive bins were also correlated. Although these features of their model fit the experimental data well, including the ray clustering effect, the Markovian nature of their model makes its use in analysis quite complex.

We now present an alternative multipath model, which is flexible enough to fit the experimental data reasonably well, while retaining the basic features of a constant-rate Poisson arrival-time process and mutually independent path gains, thus making its use in analysis relatively simple. In addition, and perhaps more importantly, the model can be explained from a physical viewpoint, thus making it more readily extendable to other types of buildings.

C. General Description of the Model

Our model starts with the physical realization that rays arrive in clusters. The cluster arrival times, i.e., the arrival times of the first rays of the clusters, are modeled as a Poisson arrival process with some fixed rate Λ. Within each cluster, subsequent rays also arrive according to a Poisson process with another fixed rate λ. Typically, each cluster consists of many rays, i.e., $\lambda >> \Lambda$.

Let the arrival time of the lth cluster be denoted by T_l, $l = 0, 1, 2, \cdots$. Moreover, let the arrival time of the kth ray measured from the beginning of the lth cluster be denoted by τ_{kl}, $k = 0, 1, 2, \cdots$. By definition, for the first cluster, $T_0 = 0$, and for the first ray within the lth cluster, $\tau_{0l} = 0$. Thus, according to our model, T_l and τ_{kl} are described by the independent interarrival exponential probability density functions

$$p(T_l \mid T_{l-1}) = \Lambda \exp\left[-\Lambda(T_l - T_{l-1})\right], \qquad l > 0, \tag{23}$$

$$p(\tau_{kl} \mid \tau_{(k-1)l}) = \lambda \exp\left[-\lambda(\tau_{kl} - \tau_{(k-1)l})\right], \quad k > 0. \tag{24}$$

Let the gain of the kth ray of the lth cluster be denoted by β_{kl} and its phase by θ_{kl}. Thus, instead of (2), our complex, low-pass impulse response of the channel is given by

$$h(t) = \sum_{l=0}^{\infty} \sum_{k=0}^{\infty} \beta_{kl} e^{j\theta_{kl}} \delta(t - T_l - \tau_{kl}). \tag{25}$$

Recall that $\{\theta_{kl}\}$ are statistically independent uniform random variables over $[0, 2\pi)$. Furthermore, the $\{\beta_{kl}\}$ are statistically independent positive random variables whose probability distributions are to be discussed in Section VII and whose mean square values $\{\overline{\beta_{kl}^2}\}$ are monotonically decreasing functions of $\{T_l\}$ and $\{\tau_{kl}\}$. In our model,

$$\overline{\beta_{kl}^2} \equiv \overline{\beta^2(T_l, \tau_{kl})} = \overline{\beta^2(0, 0)}\, e^{-T_l/\Gamma} e^{-\tau_{kl}/\gamma}, \tag{26}$$

where $\overline{\beta^2(0, 0)} = \overline{\beta_{00}^2}$ is the average power gain of the first ray of the first cluster, and Γ and γ are power-delay time constants for the clusters and the rays, respectively. A sketch that clarifies our model up to this point is given in Fig. 7.

Note that clusters generally overlap. For example, if for some k, $\tau_{kl} \geq T_{l+1} - T_l$, then the lth and the $(l+1)$th clusters overlap for all subsequent values of k. Typically, however, $\Gamma > \gamma$ and the expected power of the rays in a cluster decay faster than the expected power of the first ray of the next cluster. Thus, if $\Delta T \equiv T_{l+1} - T_l$ is sufficiently large such that $\exp[-\Delta T/\gamma] << \exp[-\Delta T/\Gamma]$, then the lth and $(l+1)$th clusters will appear disjoint.

Note also that, in principle, rays and clusters extend over an infinite time, as signified by the double infinite sum in (25). However, practically speaking, the sum over l stops when $\exp(-T_l/\Gamma) << 1$, and that over k stops when $\exp(-\tau_{kl}/\gamma) << 1$. In our room measurements, rays and clusters outside a roughly 200 ns observation window, although they exist, were in general too small to be detected.

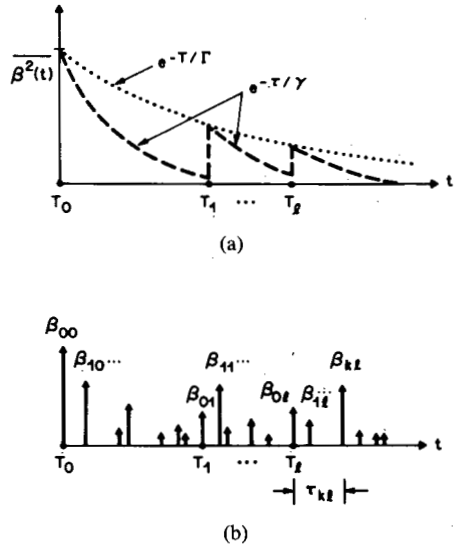

Fig. 7. A schematical representation of our model. (a) Exponentially decaying ray and cluster average powers. (b) A realization of the impulse response.

VII. Model Parameters and Physical Interpretations

A. The Cluster Arrival Rate, Λ

The first arriving cluster of rays is formed by the transmitted wave following a more-or-less "direct" path to the receiver. Such a path, which is not usually a straight line, comprises mostly open spaces (e.g., hallways), and goes through a few, but not too many, walls. Subsequent clusters result from reflections from the building superstructure (e.g., large metalized external or internal walls and doors). In our building, the two end metal doors (see Fig. 1) were the main cause of the additional clusters. Note that with this physical picture, the number and arrival times of clusters should be the same for all locations within any given room, which is what we observed experimentally.

One-half of the rooms we measured showed no evidence of additional clusters within the 200 ns observation window. (The first cluster, of course, was always present.) The other half showed, essentially, one additional relevant cluster. Using the Poisson distribution associated with (23) with a cluster arrival rate Λ, we obtain the probability of having n additional clusters in a 200 ns period as $P(n) = (200\Lambda)^n \exp(-200\Lambda)/n!$, $n = 0, 1, 2, \cdots$. We thus find that to fit our cluster observations, $1/\Lambda$ needs to be roughly in the range from 200 to 300 ns, in which case $P(0) = 0.37$ to 0.51, $P(1) = 0.37$ to 0.34, and $P(n > 1) = 0.26$ to 0.15. With only eight rooms measured, we cannot at this point be more precise in pick-

ing Λ. In Section VIII-A we will see, from another point of view, that $1/\Lambda \approx 300$ ns.

B. The Ray Arrival Rate, λ

By resolving the individual rays in about 200 power profile measurements similar to those in Figs. 3 and 4, we estimate $1/\lambda$ to be in the range of 5–10 ns. The range uncertainty comes from the fact that our ray-resolving algorithm, coupled with our measurements sensitivity, is unable to detect many weak rays, in particular, those falling near strong rays. The higher the sensitivity, the more (weak) rays we would find, and hence, the larger the value of λ. At the same time, the probability distribution of the path gains $\{\beta_k\}$ would be increased for small values of β's. Thus, the appropriate choice of λ is strongly coupled to the probability distribution of the β's. We find that a consistent choice is $1/\lambda = 5$ ns coupled with Rayleigh-distributed β's having the appropriate mean-square value (see Section VII-D). Actually, as will be discussed later (see Section VIII-B), smaller values of $1/\lambda$ could have been employed, even down to the limiting value of zero (i.e., continuous ray arrival process). This, however, is beyond our measurement time resolution.

C. The Ray and the Cluster Power-Decay Time Constants, γ and Γ

As mentioned in Section VII-A, the number of arrival times of clusters, say, $T_0, T_1, \cdots, T_L$, are the same for all locations within a given room. It follows from (26) that, within that room, the expected value of the ray power as a function of time, measured from the arrival point of the first ray of the first cluster, is given by

$$\overline{\beta^2(t)} = \overline{\beta^2(0,0)} \sum_{l=0}^{L} e^{-T_l/\Gamma} e^{-(t-T_l)/\gamma} \cup (t - T_l), \tag{27}$$

where $\cup(t)$ is the unit step function, which equals one for $t \geq 0$, and zero for $t < 0$. A sketch of (27) is shown in Fig. 7(a).

An estimate of $\overline{\beta^2(t)}$, and hence of γ and Γ, was obtained for a given room by aligning the time origin and taking the average of many measured power profiles, $s(t)$, within that room. Actually, what one obtains from this process is an estimate of the time convolution of $\overline{\beta^2(t)}$ and $p^2(t)$, the square of the transmitted pulse. However, since this pulse is narrow, the effect of the convolution is negligible. Four different examples of such space-averaged $s(t)$ are shown in Fig. 8. More than 20 power profiles were averaged in each case. Fig. 8(a) indicates that only one cluster reached the receiver in that case. Each of the remaining cases shows two arriving clusters. The time spread evident in the leading edges of a few clusters in Fig. 8 is mainly due to fundamental uncertainty in aligning the time origins of the various measured power profiles.

By fitting decaying exponentials to each cluster in Fig. 8, as well as to similar measurements taken in other rooms, we find that, on the average, rays within a cluster decay with an approximate time constant of $\gamma = 20$ ns (see dashed lines in Fig. 8). Similarly, by fitting decaying exponentials through the leading peaks of successive clusters, we find that the clusters themselves decay, on the average, with an approximate time constant of $\Gamma = 60$ ns (see dashed lines in Fig. 8).

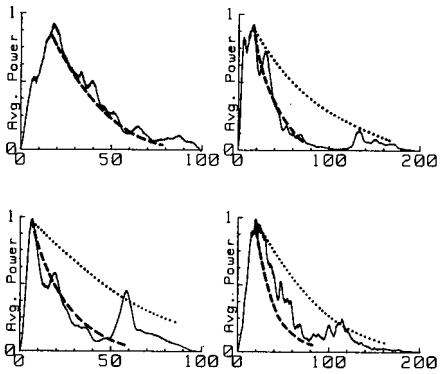

Fig. 8. Four spatially averaged power profiles within various rooms. The dashed lines correspond to exponential power decay profile of the rays and the clusters.

The use of exponentials in (26) and (27) to represent the decays of the powers of the rays and clusters as functions of time has an intuitively appealing interpretation. Consider, for example, our physical picture of the rays bouncing back and forth in the vicinity of the receiver and/or the transmitter to form a cluster. On the average, with each bounce, the wave suffers some average delay (say, equivalent to the width of a room), and some average decibels of attenuation (which depends on the surrounding materials of the walls, furnitures, etc.). In this case, the power level *in decibels* of each successive ray would be proportional to the time delay of that ray, which results in our exponential power decay characteristics. Note that from this picture, γ and Γ would be increased if the building walls were more reflective and/or if the sizes of the rooms and the building itself were increased.

D. The Probability Distribution of the Path Gains, $\{\beta_{kl}\}$

So far, our model gives the expected value of the path power gain β_{kl}^2 as a function of the associated cluster and ray delays T_l and τ_{kl}. We now make the assumption, which is reasonably supported by our observations, that the probability distribution of the normalized power gain $\beta_{kl}^2/\overline{\beta_{kl}^2}$ is independent of the associated delays, or for that matter, of the location within the building. Under this assumption, we can put the measured power gains of *all* our resolved paths into one, supposedly homogeneous, data pool by simply normalizing by the appropriate (i.e., measured within the same room and having the same delay) spatially averaged power profiles, such as those shown in Fig. 8.

The cumulative distribution of $\beta_{kl}^2/\overline{\beta_{kl}^2}$, obtained as described above, is shown by the solid line in Fig. 9. The dashed line in that figure is the unity-mean exponential

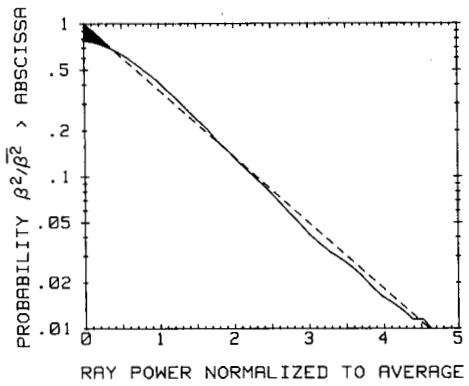

Fig. 9. Measured cumulative probability distribution of the normalized ray power for all rooms (solid line), and the best fitting exponential distribution (dashed line).

cumulative distribution, $P[\beta_{kl}^2/\overline{\beta_{kl}^2} > X] = \exp(-X)$, which appears as a straight line on the semilog plot. This results in the exponential probability density function,

$$p(\beta_{kl}^2) = (\overline{\beta_{kl}^2})^{-1} \exp(-\beta_{kl}^2/\overline{\beta_{kl}^2}), \qquad (29)$$

for the path power gain, or, equivalently, the Rayleigh probability density function,

$$p(\beta_{kl}) = (2\beta_{kl}/\overline{\beta_{kl}^2}) \exp(-\beta_{kl}^2/\overline{\beta_{kl}^2}), \qquad (30)$$

for the path voltage gain.

As mentioned earlier, our ray-resolving algorithm, coupled with our measurement sensitivity, is unable to detect many weak rays, in particular, those falling near strong rays. Thus, in fitting the unity-mean exponential cumulative distribution to the data in Fig. 9, we let the total number of resolved rays be a floating optimization parameter, instead of fixing it to the actual number observed. In effect, we let the optimization procedure estimate the number of weak rays that we could have missed. As indicated from Fig. 9, with the solid line intercepting the ordinate axis at a value of about 0.8 instead of 1, a 25 percent increase in the total number of rays is needed to achieve the best fit. This increase is reflected in the choice of λ given in Section VII-B. As can be observed from the shaded area in Fig. 9, the power of the needed rays is less than about 25 percent of the local average. Such weak rays could indeed have been missed by our ray-resolving algorithm.

It is appropriate to mention at this point that various other distributions could have fit our path gain data as well as, or even better than, the Rayleigh distribution of (30). For example, a log-normal distribution, with a standard deviation of about 4 dB, fits our data well, even without inflating the number of weak rays as was done above. However, we believe that those undetected weak rays actually exist, and that the Rayleigh distribution, which is much simpler to work with in analysis than the log-normal distribution, is quite adequate for our model.

Having rays with Rayleigh amplitudes and uniform phases, which corresponds to a complex Gaussian process, can physically occur if what we call a "ray" is actually the sum of many independent rays arriving within our time resolution. Invoking the central limit theorem then leads to the aforementioned complex Gaussian process. This is basically the same logic leading to the continuous Rayleigh model, or more precisely, the Gaussian wide-sense stationary uncorrelated scattering (GWSSUS) model of the urban mobile radio channel advocated by Bello, Cox, and others [17], [18], [12]. On the other hand, Turin and others [14]–[16] model the same channel as having discrete correlated rays with log-normal amplitudes. By comparison, our model of the indoor radio channel consists of discrete uncorrelated rays with Rayleigh amplitudes. As will be seen shortly, our model can easily be extended to a continuous model of the GWSSUS type.

VIII. Using the Model

A. Simulation Procedure

Suppose that we wish to simulate the indoor channel between a centrally located transmitter/receiver and some room at a distance r. The first step is to generate the cluster arrival times, $T_1, T_2, \cdots$, through the use of the exponential distribution of (23) with $T_0 = 0$. Before proceeding with the generation of the rays within the clusters, we need to estimate $\overline{\beta^2(0, 0)}$, the average power of the first ray of the first cluster. This quantity is directly related to the average multipath power gain $\overline{G}(r)$ for the room in question. It follows from (21), (23), and Fig. 5 that $\overline{G}(r) = G(1\text{ m})\, r^{-\alpha}$, where $G(1\text{ m})$ can be approximated by (8), and $\alpha = 3$ to 4 in our building, but can be up to 6 in other builds [2].

The relation between $\overline{G}(r)$ and $\overline{\beta^2(0, 0)}$ can be found from the definition of G in Section V-A, and from $\overline{\beta^2(t)}$, the expected value of the ray power as a function of time, given in (27). With λ being the average number of rays per unit time, it follows that[1]

$$\overline{G}(r) = \lambda \int_0^\infty \overline{\beta^2(t)}\, dt$$

$$= \gamma\lambda\, \overline{\beta^2(0, 0)} \sum_{l=0}^{L} e^{-T_l/\Gamma}. \qquad (31)$$

The summation term in (31) is usually dominated by the first term, i.e., the first cluster. For example, with T_l statistically described in (23), it can be shown that the average value of this summation is $1 + \Gamma\Lambda$. The 1 accounts for the first cluster and $\Gamma\Lambda$ accounts for subsequent clusters. In our case, with $\Gamma = 60$ ns and $1/\Lambda$ between 200 and 300 ns, this average value is between 1.3 and 1.2. Considering the ± 7 dB deviation in fitting $\overline{G}(r)$ to the power law $r^{-\alpha}$ shown in Fig. 5, the small increase (≈ 1 dB) due to subsequent clusters can safely be neglected. (Note, however, that these delayed clusters have a major

[1]Actually, more complete computation would yield (31) with $\gamma\lambda$ replaced by $(1 + \gamma\lambda)$. The added 1 accounts for the first ray of each cluster. However, usually $\gamma\lambda \gg 1$, and (31) is a valid approximation.

effect on the value of the rms delay spread.) We can finally compute $\overline{\beta^2(0, 0)}$ from

$$\overline{\beta^2(0, 0)} \approx (\gamma\lambda)^{-1} G(1 \text{ m}) r^{-\alpha} \qquad (32)$$

where $G(1 \text{ m})$ is given approximately by (8), with $r = 1$.

Now we can proceed to generate the rays within the clusters. First, the relative ray arrival times $\{\tau_{kl}\}$ are generated through the use of the exponential distribution of (24). Next, the ray amplitudes $\{\beta_{kl}\}$ are generated from the Rayleigh distribution of (30), with β_{kl}^2 given by (26). To complete the picture, the associated phase angles $\{\theta_{kl}\}$ are chosen from a uniform distribution. Depending on the application, the process of ray and cluster generation would stop when the average power of the generated rays drops below some threshold.

As mentioned in Section VII-A, we estimate the mean time between clusters in our building to be in the range $1/\Lambda = 200$–300 ns. To resolve this uncertainty, we simulated the channel as described above, computed the rms delay spread σ_τ for each simulation point, and plotted its cumulative distribution. With our other parameters being $\gamma = 20$ ns, $\Gamma = 60$ ns, and $1/\lambda = 5$ ns, the best fit to the cumulative distribution obtained directly from measurements, the solid line in Fig. 6, was for $1/\Lambda = 300$ ns. The corresponding distribution obtained from simulations is given by the dashed line in Fig. 6.

B. Discrete versus Continuous Model

Thus far, our model is presented as a discrete ray arrival process. This would be more convenient for use in studies using computer simulations. We now examine the possibility of having a continuous model.

We note that, by letting the ray arrival rate λ approach infinity, while having $\overline{\beta^2(0, 0)}$ approach zero such that their product is finite and satisfies (32), and by noting that the complex ray gains form a Gaussian process, our model mathematically approaches the continuous GWSSUS model mentioned in Section VII-D. Such a model would be more suitable for analysis [12], [17]. Some measured power delay profiles, such as the one shown in Fig. 4(d), suggest that such a continuous model might indeed represent the physical reality. On the other hand, other measurements, such as those of Fig. 3(d)–(g), which were taken on the vertices of an 0.23-m square, suggest a discrete model. This follows from the correlation evident between the various profiles, which could be attributed to three or four dominant waves traversing the observation points.

With our time resolution of about 5 ns, and with our finding of a mean time between rays of $1/\lambda \approx 5$ ns, we are unable to determine whether the indoor radio channel is best described by a discrete or a continuous model. In many studies, the answer to this question may not be relevant, while in others, the answer may be important. For example, a truly discrete model would yield a strong spatial correlation of the amplitudes of the rays received in some vicinity. This would yield some space diversity systems useless. A continuous model, on the other hand, results in the opposite conclusion. We believe from our measurements that, in most situations within the indoor channel, a continuous model or, equivalently, a high-density discrete model, is closer to the physical reality. However, as mentioned earlier, some exceptions do exist. A definitive settlement of this issue awaits future experiments involving either a better time resolution or simultaneous measurements with two or more closely spaced receiving antennas.

IX. Summary and Conclusions

We presented the results of 1.5 GHz, pulsed, multipath propagation measurements between two vertically polarized omnidirectional antennas located on the same floor within a medium-size building (AT&T Bell Laboratories, Crawford Hill location in Holmdel, NJ). A novel method of measurement was used, which involves averaging the square-law-detected received pulse response while sweeping the frequency of the transmitted pulse. This enabled us to resolve the multipath channel impulse response within about 5 ns.

Our results show the following. 1) The indoor channel is quasi-static, or *very slowly* time varying (related to people's movements). 2) The nature and statistics of the channel's impulse response is virtually independent of the states of polarization of the transmitting and receiving antennas, provided that there is no line-of-sight path between them. 3) The maximum observed delay spread in the building was 100–200 ns within rooms, with occasional delays of more than 300 ns within hallways. 4) The measured rms delay spread within rooms had a median value of 25 ns, and a maximum value of 50 ns, both being a factor of five less than those measured by Devasirvatham in a much larger building [7]. 5) The signal attenuation with no line-of-sight path varied over a 60 dB range and seems to obey an inverse distance-power law with an exponent between 3 and 4, which is in general agreement with Alexander's results [2] for this type of building.

We have also developed a simple statistical multipath model of the indoor radio channel, which fits our measurements well and, more importantly, appears to be extendable (by adjusting the values of its parameters) to other buildings. In our model, the rays of the received signal arrive in clusters. The received ray amplitudes are independent Rayleigh random variables with variances that decay exponentially with cluster delay as well as with ray delay within a cluster. The corresponding phase angles are independent uniform random variables over $[0, 2\pi)$. The clusters, as well as the rays within a cluster, form Poisson arrival processes with different, but fixed, rates. Equivalently, the clusters and the rays have exponentially distributed interarrival times. The formation of the clusters is related to the building superstructure (e.g., large metalized external or internal walls and doors). The rays within a cluster are formed by multiple reflections

from objects in the vicinities of the transmitter and the receiver (e.g., room walls, furnishings, and people).

A detailed summary of the method of using the model was given in Section VIII. Both a discrete and a continuous version of the model are possible. The former is more suitable for computer simulations, while the latter would be more desirable in analysis.

Acknowledgment

We thank Prof. P. J. McLane for many stimulating discussions, especially about the discrete versus continuous multipath models. We also thank L. J. Greenstein, D. J. Goodman, and M. M. Kavehrad for their useful suggestions and comments, and R. A. Semplak and G. J. Owens for their design of the discone antennas used in the experiment. We also acknowledge the valuable contributions of R. D. Nash in the early phase of the experiment, and the able help of M. F. Wazowicz in maintaining the equipment. Last, but not least, we thank T. A. Saleh and O. A. Saleh for their help in the tedious task of gathering the valuable experimental data.

References

[1] S. E. Alexander, "Radio propagation within buildings at 900 MHz," *Electron Lett.*, vol. 18, no. 21, pp. 913–914, Oct. 14, 1982.

[2] S. E. Alexander, "Characterizing buildings for propagation at 900 MHz," *Electron Lett.*, vol. 19, no. 20, p. 860, Sept. 29, 1983.

[3] H. H. Hoffman and D. C. Cox, "Attenuation of 900 MHz radio waves propagating into a metal building," *IEEE Trans. Antennas Propagat.*, vol. AP-30, pp. 808–811, July 1982.

[4] D. C. Cox, R. R. Murray, and A. W. Norris, "Measurements of 800 MHz radio transmission into buildings with metallic walls," *Bell Syst. Tech. J.*, vol. 62, no. 9, pp. 2695–2717, Nov. 1983.

[5] ——, "800 MHz attenuation measured in and around suburban houses," *AT&T Bell Lab. Tech. J.*, vol. 63, no. 6, pp. 921–954, July–Aug. 1984.

[6] D. M. J. Devasirvatham, "Time delay speed measurements of 850 MHz radio waves in building environments," in *GLOBECOM '85 Conf. Rec.*, vol. 2, Dec. 1985, pp. 970–973.

[7] ——, "The delay spread measurements of wideband radio signals within a building," *Electron. Lett.*, vol. 20, no. 23, pp. 950–951, Nov. 8, 1984.

[8] A. G. Kandoian, "Three new antenna types and their applications," *Proc. IRE*, vol. 34, no. 2, pp. 70W–75W, Feb. 1946.

[9] J. G. Proakis, *Digital Communications*. New York: McGraw-Hill, 1983, ch. 7.

[10] S. Ramo, J. R. Whinnery, and T. Van Duzer, *Fields and Waves in Communication Electronics*. New York: Wiley, 1965, p. 717, eq. (7).

[11] D. C. Cox, "Delay Doppler characteristics of multipath propagation at 910 MHz in a suburban mobile radio environment," *IEEE Trans. Antennas Propagat.*, vol. AP-20, pp. 625–635, Sept. 1972.

[12] B. Glance and L. J. Greenstein, "Frequency selective fading effects in digital mobile radio with diversity combining," *IEEE Trans. Commun.*, vol. COM-31, pp. 1085–1094, Sept. 1983.

[13] H. F. Schmid, "A prediction model for multipath propagation of pulse signals at VHF and UHF over irregular terrain," *IEEE Trans. Antenna Propagat.*, vol. AP-18, pp. 253–258, Mar. 1970.

[14] G. L. Turin, F. D. Clapp, T. L. Johnston, S. B. Fine, and D. Lavry, "A statistical model of urban multipath propagation," *IEEE Trans. Veh. Technol.*, vol. VT-21, pp. 1–9, Feb. 1972.

[15] H. Suzuki, "A statistical model for urban radio propagation," *IEEE Trans. Commun.*, vol. COM-25, pp. 673–680, July 1977.

[16] H. Hashemi, "Simulation of the urban radio propagation channel," *IEEE Trans. Veh. Technol.*, vol. VT-28, Aug. 1979.

[17] A. P. Bello and B. D. Nelin, "The effect of frequency selective fading on the binary error probability of incoherent and differentially coherent matched filter receivers," *IEEE Trans. Commun. Syst.*, vol. CS-11, pp. 170–186, June 1963.

[18] D. C. Cox and R. P. Leck, "Correlation bandwidth and delay spread multipath propagation statistics for 910 MHz urban mobile radio channels," *IEEE Trans. Commun.*, vol. COM-23, pp. 1271–1280, Nov. 1975.

[19] R. R. Murray, H. W. Arnold, and D. C. Cox, "815 MHz radio attenuation measured within a commercial building," in *Dig. 1986 IEEE Int. Symp. Antennas Propagat.*, vol. 1, June 1986, pp. 209–212.

[20] D. M. J. Devasirvatham, "A comparison of time delay spread measurements within two dissimilar office buildings," in *ICC'86 Conf. Rec.*, vol. 2, June 1986, pp. 852–857.

Adel A. M. Saleh (M'70–SM'76–F'87) was born in Alexandria, Egypt, on July 8, 1942. He received the B.Sc. degree in electrical engineering from the University of Alexandria, Alexandria, Egypt, in 1963, and the M.S. and Ph.D. degrees in electrical engineering from the Massachusetts Institute of Technology, Cambridge, in 1967 and 1970, respectively.

From 1963 to 1965 he worked as an Instructor at the University of Alexandria. In 1970 he joined AT&T Bell Laboratories, Holmdel, NJ, where he is engaged in research on microwave and optical components and communications systems.

Dr. Saleh is a member of Sigma Xi.

Reinaldo A. Valenzuela (M'85) received the B.Sc.(Eng.) degree from the School of Engineering, University of Chile, in 1977. He received the Ph.D. degree in 1982 through the study of "techniques for transmultiplexer design."

From 1975 to 1977 he worked for Thomson-CSF (Chile) in the setting-up and commissioning of large telecommunication networks. In 1978 he joined the Department of Electrical Engineering, Imperial College, London, England, where, in 1981, he was appointed a Research Assistant, sponsored by British Telecom for the study of digital filters for CODEC applications. He then joined DATABIT Ltd. (U.K.) where he participated in the analysis and design of a full duplex, echo cancelling system for the transmission of 88 kbits/s data and analog voice signals over the subscriber loop. Since 1984 he has been a member of the Communications Methods Research Department, AT&T Bell Laboratories, Holmdel, NJ, where he has been studying local area networks issues such as indoor microwave propagation and the integration of voice and data in multiple access packet networks.